Final Report on

Assessing the Far Field Effects of Tidal Power Extraction on the Bay of Fundy, Gulf of Maine and Scotian Shelf

Grant Recipients: Jinyu Sheng[1], Keith Thompson[1], Dave Greenberg[2], Paul Hill[1]

[1]Department of Oceanography, Dalhousie University, Halifax, NS, B3H 4J1
[2]Bedford Institute of Oceanography, Dartmouth, NS, B2Y 4A2

Starting period: January 1, 2010
Reporting period: January 1, 2010 to May 31, 2012
Submitted on: June 11, 2012

Summary

The Bay of Fundy and Gulf of Maine system has a natural resonant period very close to the main semi-diurnal lunar tide. This results in the world's highest tides and strong tidal currents in the Bay of Fundy, particularly in Minas Channel and Minas Basin. The physical and ecological conditions in the "far field" could undergo significant changes given significant extraction of tidal power from this near-resonant system. The "far-field" in this project includes the Bay of Fundy (BoF) and adjacent Gulf of Maine (GoM) and western Scotian Shelf (SS). This research project is to quantify the far-field effects of tidal power extraction with a particular focus on tides, tidal current patterns, the vertical and horizontal distribution of temperature and salinity and also large-scale sediment distributions from numerical results produced by ocean circulation models.

Two types of ocean circulation models based on the Princeton Ocean Model (POM) were used in this study. The first is the three-dimensional (3D), barotropic tidal circulation model for examining the far-field effect of tidal energy extraction in the Minas Passage on the tidal elevations and 3D tidal currents in the BoF-GoM system. The tidal in-stream energy extraction in the model is parameterized in terms of the quadratic Rayleigh friction in the momentum equation. A suite of numerical experiments are conducted to determine the ranges of extractable tidal in-stream energy and resulting effects on the 3D tidal circulation in the BoF-GoM region in terms of the Rayleigh friction coefficients. The 3D model results suggest that the maximum energy extraction in the Minas Passage increases tidal elevations and tidal currents throughout the GoM and reduces tidal elevations and circulation in the upper BoF, especially in the Minas Basin. The far-field effect of tidal energy extraction in the Passage on the 3D tidal circulation in the BoF-GoM region is examined in two cases of harnessing tidal in-stream energy from (a) the entire water column and (b) the lower water column within 20 m above the bottom in the Passage. It was found that tidal in-stream energy extraction from the lower water column has must less impact on the tidal elevations and circulation in the BoF-GoM than the energy extraction from the whole water column in the Minas Passage.

The second type of the circulation models used in the study is the 3D shelf circulation forecast model known as DalCoast for investigating the far-field effect of the tidal energy extraction on the 3D total currents (including tidal, wind-driven and density-driven currents) and temperature/salinity fields in the BoF, GoM, and western SS. DalCoast was integrated for one year and model results were used to generate the monthly and annual means of currents and hydrographic distributions. It was found that the tidal energy extraction in the Minas Passage affects significantly the monthly and annual mean circulation and hydrographic distributions in the BoF, particularly in the inner BoF. The maximum tidal energy extraction in the Minas Passage also has some noticeable effects in the density-driven currents and temperature/salinity distributions over the central GoM and western SS.

The far-field effect of the tidal energy extraction on the bottom sediment properties was also studied based on the maximum bed shear stress calculated from the near bottom maximum tidal currents. In case B, the significant effect of tidal energy extraction on the large-scale distribution of the near-bottom sediment occurs mainly over the BoF.

Scientific Objectives

The main objective of this project is to quantify the far-field effects of tidal power extraction with a particular focus on tides, the tidal current patterns, the vertical and horizontal distribution of temperature and salinity and also large-scale sediment distributions.

Main Research Results

Significant research results were obtained in quantifying the far-field effects of tidal extraction in the Minas Passage on (a) the 3D tidal circulation, (b) 3D general circulation and hydrographic distributions and (c) sediment distributions in the Bay of Fundy (BoF), Gulf of Maine (GoM) and Scotian Shelf (SS).

(a) Far-field effects on tidal circulation in the BoF-GoM region

For examining the far-field effect of tidal energy extraction in the Minas Passage on the 3D tidal circulation in the BoF and GoM, a two-level nested-grid tidal circulation model was developed for the BoF-GoM system using the parallel version of the Princeton Ocean Model (POM) with the drying-wetting lateral boundary condition. The nested-grid BoF-GoM tidal circulation modelling system has a coarse-resolution (~3.5 km) parent sub-model covering the GOM and a fine-resolution (~1.5 km) child sub-model covering the BoF (Figure 1). A two-way nesting technique was used for exchanging information between the parent and child sub-models over the dynamic overlapping area of the two sub-models (Hasegawa et al., 2011). The quadratic Rayleigh friction formulation was used in the model to represent the turbine drag in the 3D momentum equation.

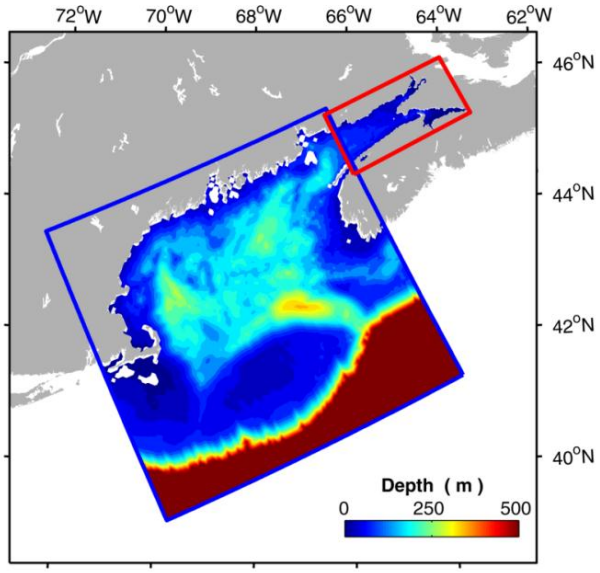

Figure 1. *Major topography (image) and domains of the two-level nested-grid tidal circulation model developed for the Bay of Fundy and Gulf of Maine region. The region marked by the blue box is the domain of the parent sub-model and the region marked by the red box is the domain of the child sub-model. The narrow zone marked by both the red and blue lines represents the dynamic interface between the parent and child sub-models where the two-way nesting technique is used.*

Model validation is an essential step in any modelling work. To assess the performance of the BoF-GoM tidal circulation model, the tidal model was first used to simulate tidal surface elevations and 3D tidal currents in the BoF-GoM without turbine drag (control run). Amplitudes and phases of three major tidal constituents N_2, N_2, and S_2 were calculated from model results in the control run. The spatial distributions of co-amplitudes and co-phases of M_2 and N_2 in the BoF-GoM region in the control run (Figures 2 and 3) are in good agreement with previous numerical results (Sucsy et al., 1993; Dupont et al., 2005). The tidal elevations at the 10 tide gauges produced by the BoF-GoM tidal model agree with the observations and WebTide (Figures 2 and 3). (WebTide is a simple tidal prediction program based on pre-calculated major tidal constitutes over the region (Dupont et al., 2005)).

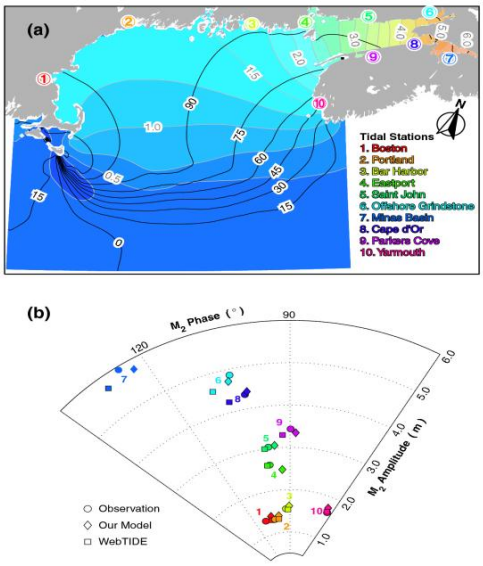

Figure 2. *Co-amplitudes (image with gray contour lines) and co-phases (black contour lines) of simulated M_2 constituent (upper panel) surface elevations produced by the BoF-GoM tidal model in the control run. The contour intervals are 0.25 m for amplitude and 15◦ for phase. Lower panel shows amplitude-phase polar plot of observed (circles) and simulated (diamonds) surface elevations at ten tide locations marked by circled numbers in top panels. For comparison, the WebTide results (squares) are also shown.*

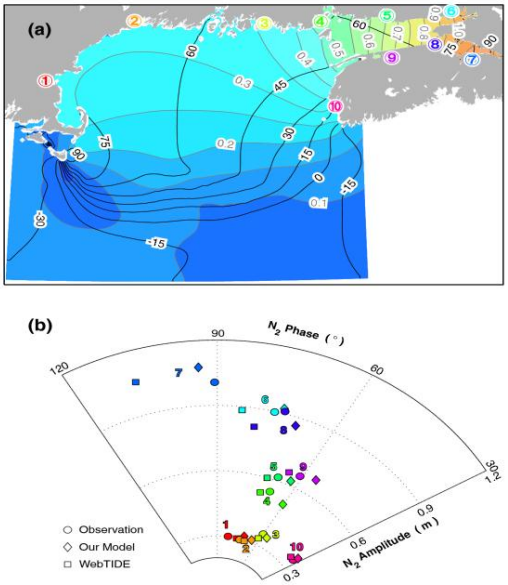

Figure 3. *Same format as in Figure 2, but for N_2 constituent.*

The nested-grid tidal model with the Rayleigh parameterization of the turbine drag was used to study the 3D circulation affected by in-stream power extraction to take place at any depth of the water column over the Minas Passage marked in Figure 4. Two special cases were considered (Figure 5). In case A, the tidal in-stream energy extraction takes place in the whole water column over the central area of the Minas Passage. In case B, the tidal energy extraction takes place only in the lower water column within 20 m from the bottom.

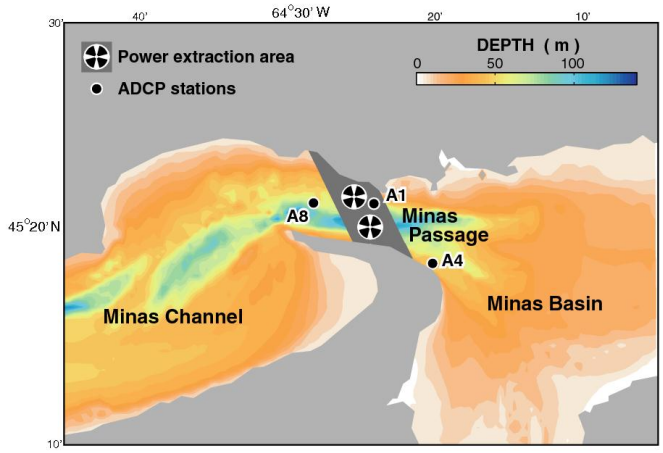

Figure 4. *Map showing the tidal in-stream power extraction area (a dark gray-shaded area) in the Minas Passage as specified in the child sub-model.*

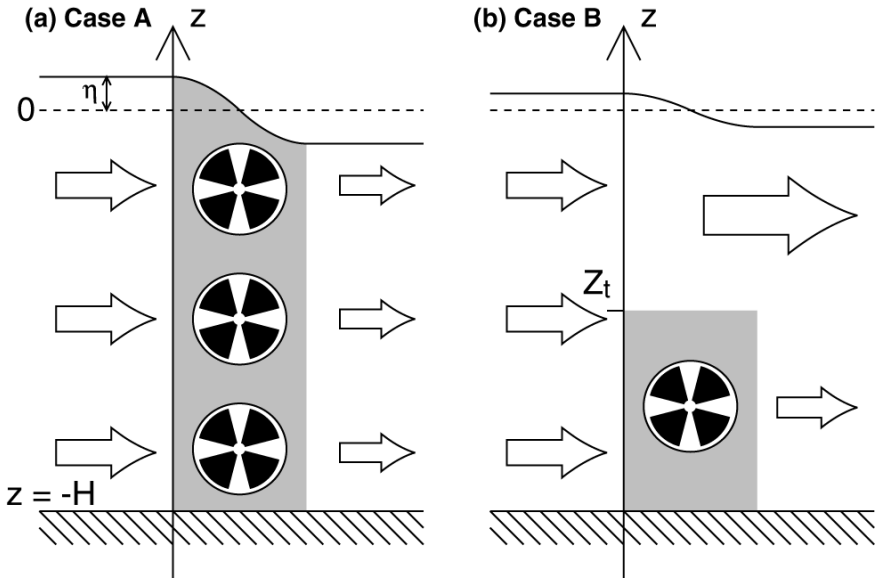

Figure 5. *Schematic showing turbine configurations for harvesting in-stream energy in the Minas Passage from (a) the entire water column in case A, and (b) the lower half of the water column in case B.*

The time-mean total tidal kinetic energy (P_{avg}) available for extraction from tidal currents in the Minas Passage calculated from model results (Figure 6a) differs in the two cases. In case A (in which the tidal in-stream energy extraction is taken from the whole water column in the Minas Passage), P_{avg} increases with the normalized turbine drag coefficient γ^* (i.e., adding more turbines in the Minas Passage) (Figure 6a). After reaching the maximum time mean extractable power of about ~7.1 GW at γ^*=~0.18, P_{avg} decreases with the increase of the turbine drag because too many turbines will block the tidal flow, which is consistent with a theoretical study based on 2D dynamics by Garrett and Cummins (2004). By comparison, in case B (in which the in-stream energy extraction is taken from the lower water column in the Minas Passage), the time-mean tidal kinetic energy also increases with γ^* but with a more gentle slope for γ^*<0.18, and reaches the maximum value of ~2 GW at γ^*=~0.66 (Figure 6a). Therefore, we consider the situation with γ^* =0.18 and P_{avg} = 1.6 GW to be the extreme scenario for the tidal energy extraction in case B.

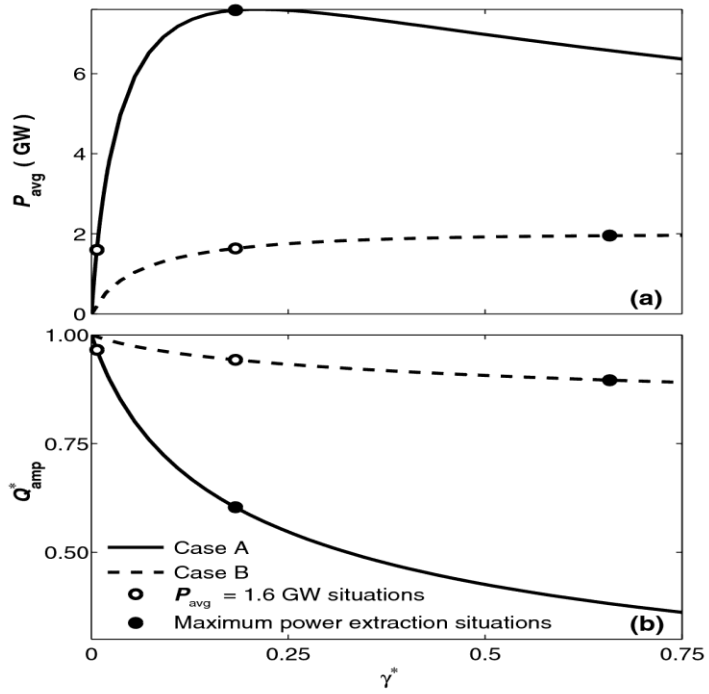

Figure 6. *(a) Time-averaged tidal power extraction rate P_{avg} in the Minas Passage and (b) Normalized M_2 along-channel flow volume amplitude (Q_{amp}) as a function of normalized turbine drag coefficient (γ^*). Solid and dashed lines represent model results by extracting the tidal in-stream energy from the entire water column (case A) and from the lower water column (case B) from the Minas Passage.*

For γ^* << 0.18 the changes in amplitudes and phases of tidal elevations in case A are small in the study region except for the upper BoF (Figure 7). At γ^* = 0.18 there are significant decreases in amplitudes of the three major tidal constituents in the upper BoF and moderate increases over the western GoM. In the upper BoF, the maximum decrease in the tidal surface elevation amplitudes is about 2.4 m for M_2, 0.49 m for N_2, and 0.43 m for S_2 in case A with γ^* = 0.18 (Figure 7). The maximum amplitude increase of about 0.2 m in the M_2 surface elevations occurs over Massachusetts Bay and adjacent coastal waters of the western GoM in this case; and small amplitude increases of less than 4 cm for N_2 and S_2 occur over the coastal waters of the western GoM.

The extreme situation in case B has a small impact on the tidal surface elevations over the study region. Figure 8b shows that, in case B with γ^*= 0.18, the maximum amplitude decreases in the upper BoF is up to 0.36 m for the M_2 surface elevations while the maximum amplitude increase is about 0.02 cm for the M_2 tidal surface elevations over Massachusetts Bay and the adjacent coastal waters of the western GoM. The effects on the N_2 and S_2 constituents are even smaller in case B with the same γ^* values (not shown). The effect of 0.4 GW power gain from 1.6 GW (γ^*=0.18) to 2.0 GW (γ^*= 0.66) in case B leads to almost double the relative change of the M_2 surface elevation amplitude (Figure 8b, c), and the effect of halving the power utilization from 1.6 GW (γ^* = 0.18) to 0.8 GW (γ^*= 0.04) results in two thirds less impact on the M_2 surface elevation change in the Minas Basin (Figure 8a, b).

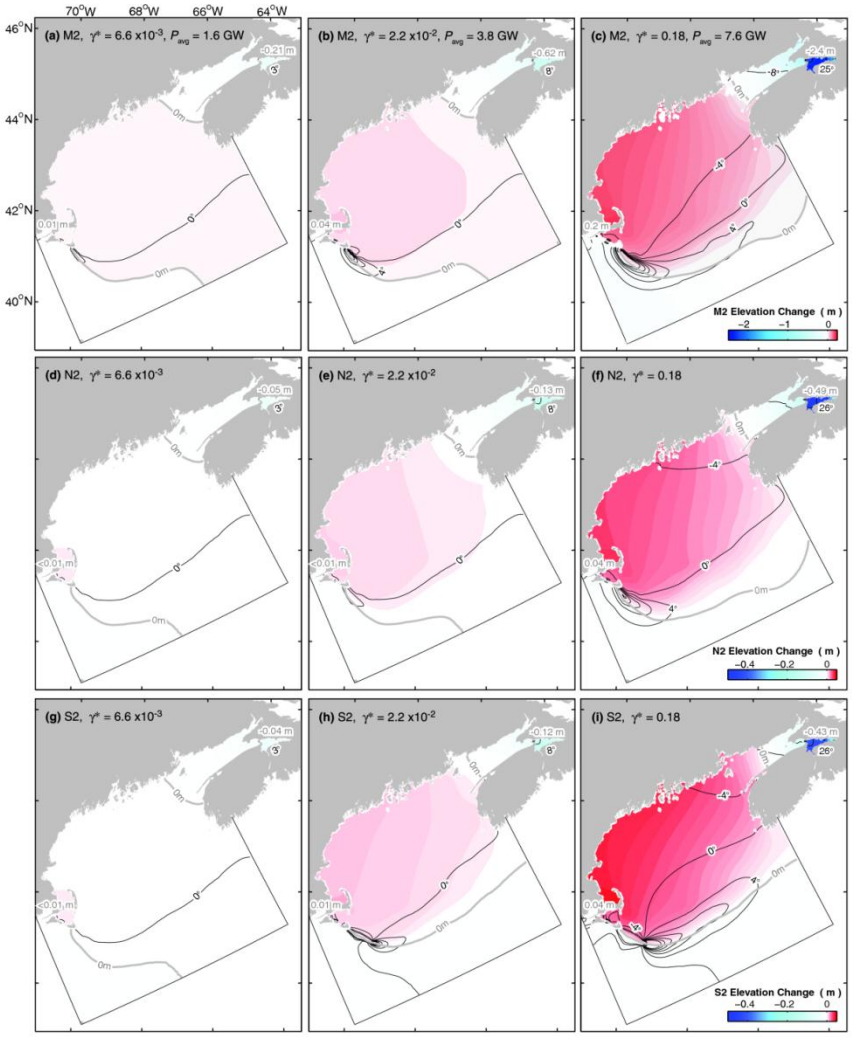

Figure 7. *Changes (case A—control) in amplitude (color shading and light gray contour lines) and phases (black contour lines) of modeled M_2 (upper panels), N_2 (middle panels), and S_2 (lower panels) surface elevations associated with different values of turbine drag coefficients in case A.*

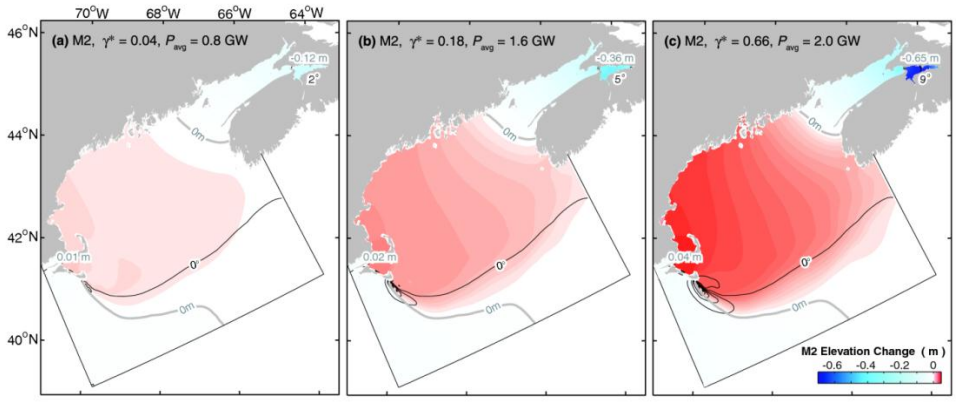

Figure 8. *Changes (case B-control run) in amplitudes (color shading and light gray contour lines) and phases (black contour lines) of modeled M_2 surface elevations associated with different values of turbine drag coefficients in case B.*

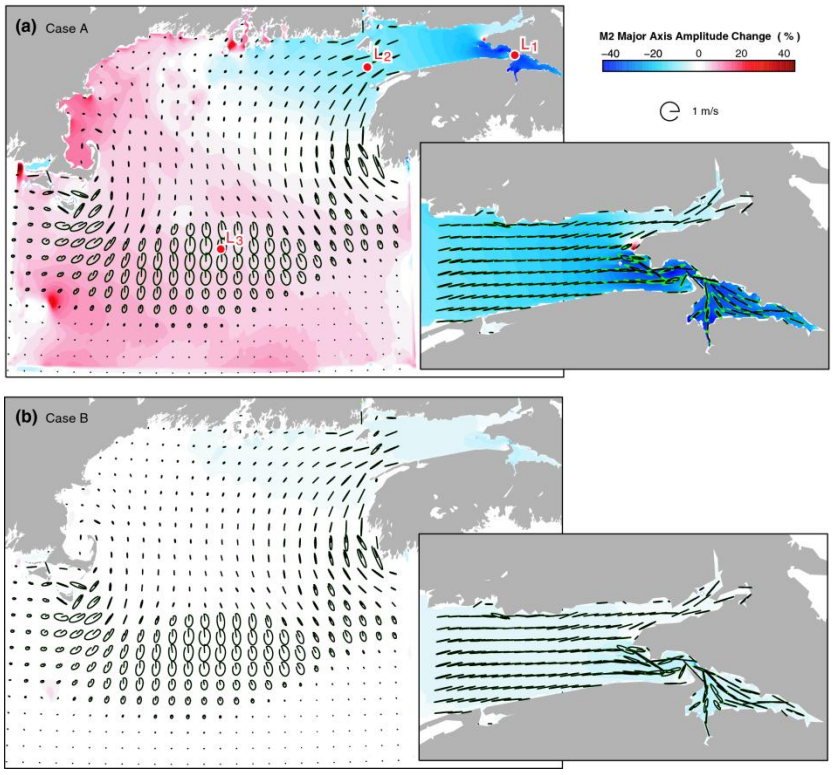

Figure 9. *The M_2 tidal current ellipses (black) and major axis amplitude change (color shading) for tidal in-stream energy taken due to (a) case A with the maximum power extraction and (b) case B with extreme power extraction. The green ellipses shown under the black ellipses represent the model results in the control run (no energy extraction).*

The depth-mean tidal current ellipses without energy extraction in the control run are nearly rectilinear in the BoF and more circular on the Georges Bank, Nantucket Shoals and Brown Bank to the southwest of Yarmouth (Figure 9). The M_2 tidal currents are relatively strong in the BoF and over shallow regions including Nantucket Shoals, Georges Bank, Brown Bank and coastal waters around Yarmouth. The strongest tidal jet of about 4 m/s produced by the model occurs in the Minas Passage. With the maximum power extraction from the whole water column in the Passage in case A, the M_2 tidal current speeds reduce over the entire BoF by up to 40%, and increase in general over the entire GoM (Figure 9a). By comparison, the tidal extraction from the lower water column in the central Passage in case B has a much smaller effect on the tidal circulation in the GoM, with some small velocity changes in the BoF and coastal waters over the western GoM (Figure 9b).

Figure 10 shows the major axis amplitude and phase of the M_2 tidal current ellipses at site L1 in the Minas Passage (its position is shown in Figure 9) in the three cases. In case A, the major axis amplitude of M_2 decreases and the phase increases with the increase of the turbine drag throughout the water column (Figure 10a,b). By comparison, in case B, the major axis of M_2 at site L1 in the lower water column decreases with stronger vertical shear (Figure 10c) as the turbine drag increases. It is interesting to note that the M_2 tidal currents in the upper surface layer at site L1 in case B are stronger for larger turbine drag coefficients than the control run (i.e., zero turbine drag), indicating that the tidal flow in the lower water column at L1 has a tendency to be steered by the turbine and then joins the free stream above the turbine. The tidal in-stream energy extraction in the Minas Passage also affects the 3D tidal circulation in the areas far from the energy extraction area. Figure 11 presents vertical profiles of M_2 current major axis amplitudes and phases at site L2 near the mouth of the BoF and site L3 on Georges Bank. Similar logarithmic velocity profiles occur at sites L2 and L3 for cases A and B. At site L2 near the mouth of the BoF, there is about 12% reduction for case A (Figure 11a) and about 2% of flow reduction for case B, in comparison with model results in the control run. At site L3 on Georges Bank, there is about 5% flow deceleration in case A, in comparison with the control run. The model results for case B are almost identical with these in the control run at this site (Figure 11c). There are some phase differences at site L3 in the two cases in comparison with the control run.

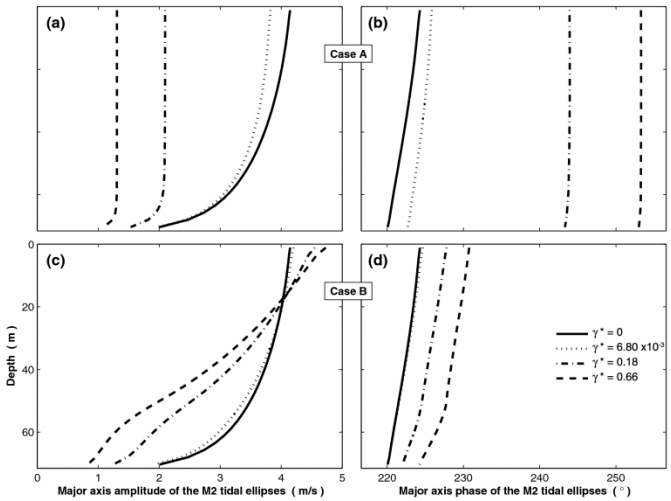

Figure 10. *Vertical profiles of the major axis amplitudes (left panels) and phases (right panels) of the M_2 tidal currents at site L1 in Minas Passage (see Figure 9 for location) for case A (upper panels) and from the lower water case B (lower panels) with four different Rayleigh velocity friction coefficients of $\gamma^* = 0$ (control run), $\gamma^* = 6.8 \times 10^{-3}$, 2.2×10^{-2}, 0.18 and 0.66.*

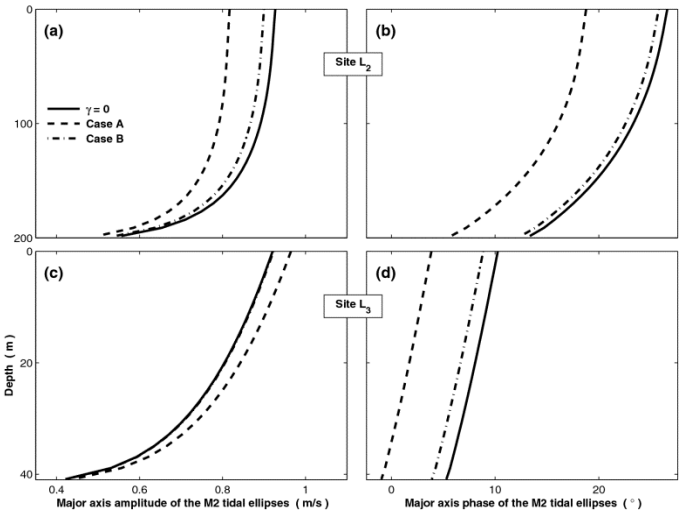

Figure 11. *Vertical profiles of major axis amplitudes (left panels) and phases (right panels) of the M_2 tidal currents at site L2 near the mouth of the Bay of Fundy (upper panels) and at site L3 on Georges Bank (lower panels) with Rayleigh velocity friction coefficients of $\gamma^* = 0$ (control run) and 0.18 in cases A and B.*

(b) Far-field effects on general circulation and hydrography in the BoF-GoM-SS region

The shelf circulation forecast model known as DalCoast was used for examining the far-field effects of tidal in-stream energy extraction in the Minas Passage on the 3D general circulation (including wind-driven, tidal and density-driven currents) and temperature/salinity distributions in the BoF, GoM and western SS. Dalcoast was chosen here since the model can be driven by various external forcing functions including wind, tides, the net sea-surface heat and freshwater fluxes, and freshwater discharge from rivers (Thompson et al., 2007; Ohashi et al., 2009a; Ohashi et al., 2009b).

The default setup of DalCoast has a 3D circulation model (inner model) covering the Gulf of St. Lawrence, Scotian Shelf and the eastern part of the BoF-GoM region, which is nested inside a large-scale storm surge model (outer model) for the eastern Canadian Shelf from Labrador Shelf to the Gulf of Maine. For this study, significant efforts were made to upgrade the inner model of DalCoast in three aspects: (a) extending the inner model domain to cover the whole BoF and GoM; (b) specification of net surface heat and freshwater fluxes; and (b) specification of freshwater runoff from major rivers in the region. Figure 12 presents the domain of the modified inner model of the DalCoast and names of major rivers and idealized narrow channels to represent the rivers. Freshwater discharge of each river is specified at the head of the idealized channel based on the monthly mean climatology of river discharge. The time steps used in the inner model of DalCoast are 9 sec for the external mode and 180 sec for the internal mode of the POM.

Both the inner and outer models of DalCoast were driven by the atmospheric forcing including wind and atmospheric pressure at the sea level taken from 3-hourly North American Regional

Reanalysis (NARR) fields. The horizontal resolution of the NARR fields is 32 km. The inner model was also forced by tidal forcing specified at the model open boundaries based in WebTide. The net heat and freshwater fluxes at the sea surface of the inner model were calculated using the NARR fields and the model sea surface temperature and salinity. As mentioned above, freshwater discharges from major rivers in the region including the St. Lawrence River and St. John River are included as the external forcing for the inner model. The combination of the spectral method (Thompson et al., 1997) and the semi-prognostic method (Sheng et al., 2001) was used in the inner model to reduce the model seasonal drift.

The performance of the inner model of DalCoast in simulating storm surges, tidal circulation and baroclinic circulation has been extensively validated in the past (Thompson et al., 2007; Ohashi et al., 2009a; Ohashi et al., 2009b). Figure 13 demonstrates, for example, that DalCoast simulates reasonably well the sub-tidal sea level elevations at Rimouski of the Gulf St. Lawrence in the fall of 2002. Ohashi et al. (2009a) recently demonstrated that the inner model of DalCoast also has satisfactory skill in simulating tidal currents in the study region based on the good agreement between the observed and simulated tidal currents at three sites in the GSL and SS (Figure 14).

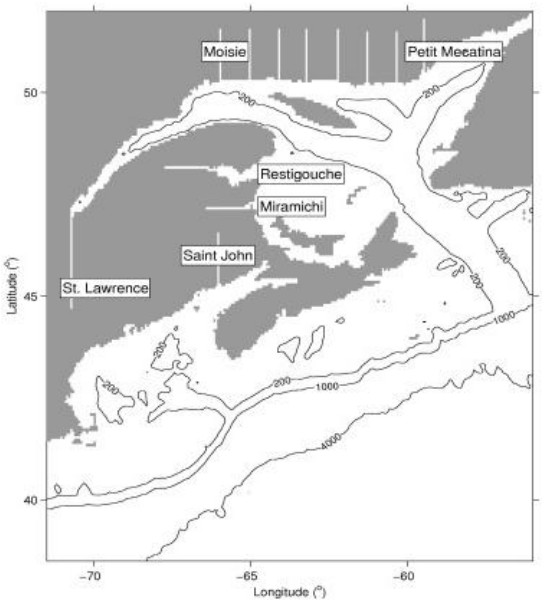

Figure 12. *The inner model domain of the shelf circulation forecast system known as DalCoast and names of major rivers (marked by black boxes) in the GSL-SS-BoF-GoM region (Courtesy of Kyoko Ohashi).*

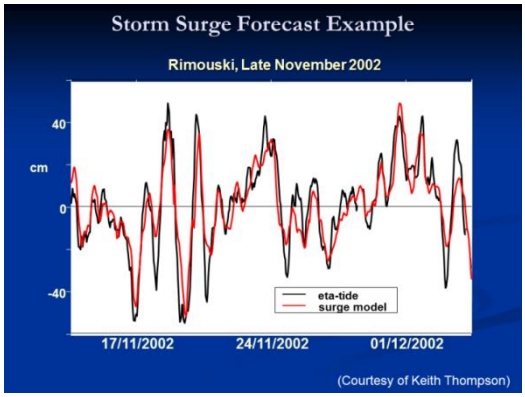

Figure 13. *Comparison of observed (red) and simulated storm surge surface elevations at Rimouski of the Gulf St. Lawrence in November and December of 2002.*

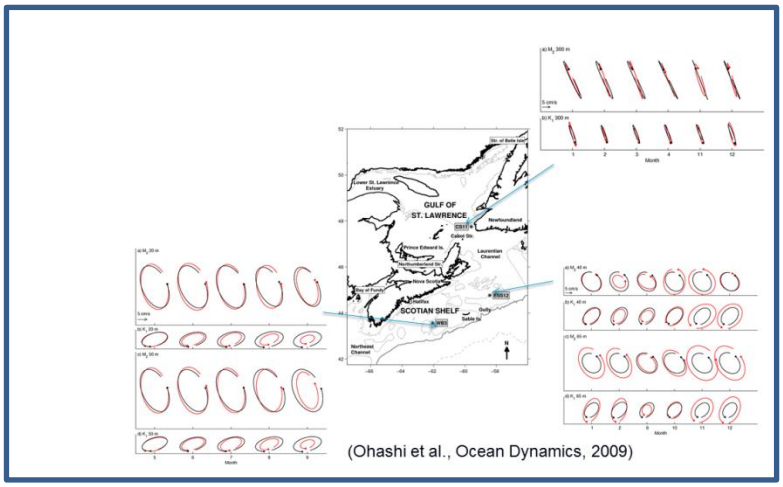

Figure 14. *Comparison of observed (red) and simulated (black) tidal currents at sites of CS11 on Cabot Strait (upper right), WBC over Western Bank (lower left) and ESS2 on Banquereau Bank (lower right) (Ohashi et al., 2009a).*

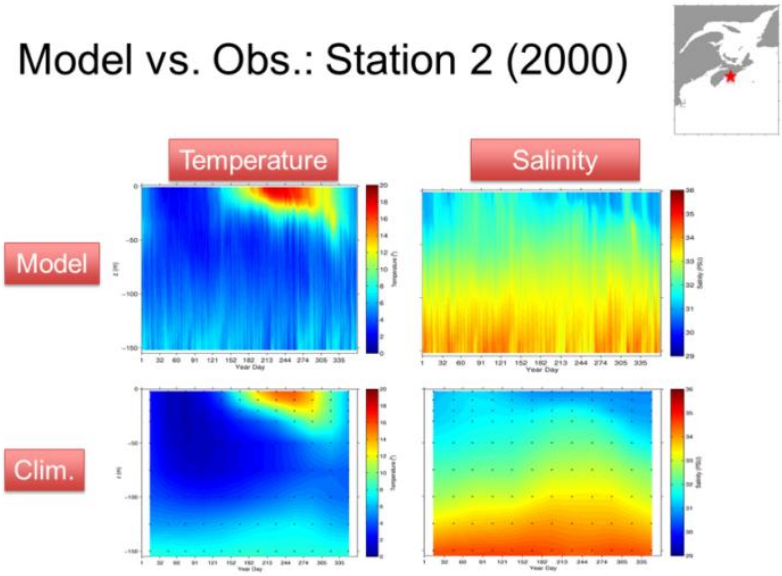

Figure 15. *Comparison of simulated (upper panels), monthly mean climatological (lower) temperature (left) and salinity (right) in 2000 at station 2 of Halifax line (Courtesy of Kyoko Ohashi).*

A comparison of simulated temperature and salinity with the monthly climatology of hydrography produced by Geshelin et al. (1999) at station 2 of the Halifax Line is shown in Figure 15, which demonstrates that the inner model of DalCoast generates reasonably well the seasonal variations and vertical distributions of temperature and salinity at the station, in comparison with the monthly mean climatology. The inner model also generates reasonably well the high-frequency variability in the temperature and salinity fields (Figure 15).

Three different numerical experiments were conducted to examine the far-field effects of tidal energy extraction in the Minas Passage on the 3D circulation and temperature/salinity distributions. In the first experiment, DalCoast was integrated for one year from January 1, 1999 without energy extraction (Control Run, Exp-CR). In the second and third experiments, DalCoast was also integrated for one year from January 1, 1999, but with the in-stream energy extraction in case A (Exp-A) and in case B (Exp-B). Same as before, in case A the tidal in-stream energy extraction takes place in the whole water column over the central area of the Minas Passage. In case B, the tidal energy extraction takes place only in the lower water column within 20 m from the bottom. The quadratic Rayleigh friction coefficient (γ^*) was set to be 0.084 in Exp-A and 0.1 in Exp-B.

To examine the far-field effects on the circulation and hydrography on the low-frequency band, monthly mean circulation and temperature/salinity fields were calculated from instantaneous model results. Figures 16 and 17 present the monthly mean sea-surface currents, temperature and salinity produced by the inner model in May and August over the BoF, GoM, and western SS. In comparison with previous numerical studies for this region (e.g., Lynch et al., 1996; Xue et al., 2000), the inner model of DalCoast simulates reasonably well the seasonal variations of sea-surface temperature and salinity. DalCoast generates a band of cold surface temperature over the inner western SS, along the coastline of eastern Maine and outer BoF, which agrees with the satellite remote sensing SST (e.g., Pettigrew et al., 1998). This band of cold surface waters, particularly in summer months, are mainly associated with coastal upwelling due to the alongshore wind forcing.

The monthly mean sea surface salinity shown in Figure 17 features relatively fresh surface waters over the coastal waters of the western SS, northwestern GoM and BoF, particularly coastal waters around the mouth of the St. John River. The monthly mean sea surface salinity in Exp-CR also has noticeable month-to-month variability (Figure 17).

The differences in the monthly mean currents (Δu) and temperature/salinity (ΔT and ΔS) between Exp-A and Exp-CR are used to quantify the far-field effect of the tidal in-stream energy extraction in the Minas Passage on the general circulation and hydrography over the BoF-GoM-SS region. Figure 18 demonstrates that the differences in currents and hydrography are relatively small in the study region except for the inner BoF, central GoM and Browns Bank on the southwestern SS. In comparison with the monthly mean sea surface temperature in Exp-CR, the May and August mean sea surface temperatures in Exp-A are warmer of about 2^oC over the Minas Passage and Basin of the inner BoF and slightly warmer of about 0.5^oC over the Georges Basin on the central GoM. It should be noted that relatively large differences in the monthly mean sea surface salinity between Exp-A and Exp-CR occur mainly in the central GoM and the southwestern SS.

Figure 19 presents the differences between Exp-A and Exp-CR at 50 m. Similar to the differences at the sea surface, large differences in the currents and hyrography at 50 m also occur over the central GoM and southwestern SS.

The differences in the annual mean currents and temperature/salinity between Exp-A and Exp-CR shown in Figure 20 have similar spatial distributions and relatively small everywhere except

for the regions of the Minas Passage and Basin, outer BoF, central GoM, and southwestern SS. The differences in the monthly and annual mean currents and hydrography between Exp-B and Exp-CR at the sea surface and 50 m shown in Figures 21-23 have similar horizontal features as the differences between Exp-A and Exp-CR, with relatively large differences over the Minas Passage and Basin, outer BoF, central GoM, and southwestern SS.

It can be argued based on the differences shown in Figures 16-23 that significant in-stream kinetic energy extraction in the Minas Passage does not affect significantly the monthly mean currents over the study region, except for the Minas Passage and Basin, outer BoF, Georges Basin on the central GoM, and Browns Bank on the southwestern SS. Although exact physical reasons for relatively large differences over these areas are not clear, it is likely due to the change in the large-scale density circulation and tidal mixing in the region affected by the significant energy extraction in the Minas Passage. It should be noted that the ecosystem dynamics in the BoF and GoM are sensitive to the tidal circulations, tidal mixing, large-scale density-driven currents and temperature/salinity distributions. The issue how the ecosystem dynamics in the region will be affected by the tidal in-stream energy extraction in the Minas Passage is very interesting and important but beyond the scope of this study.

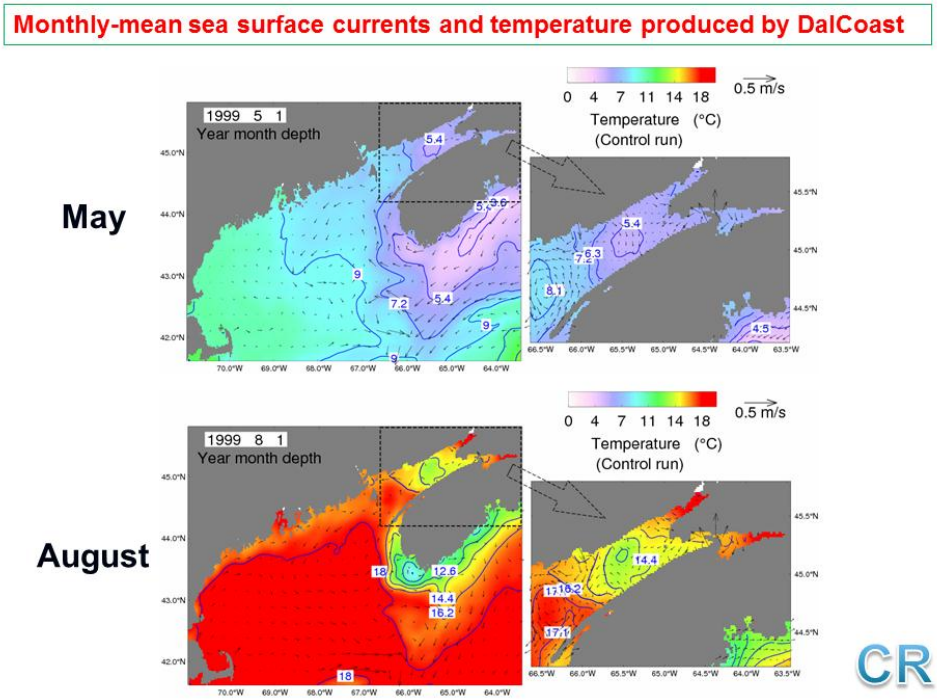

Figure 16. *Monthly mean sea surface temperature in May (upper panels) and August (lower panels) over the BoF, GoM and western SS produced by DalCoast in control run (without tidal in-stream energy extraction, Exp-CR).*

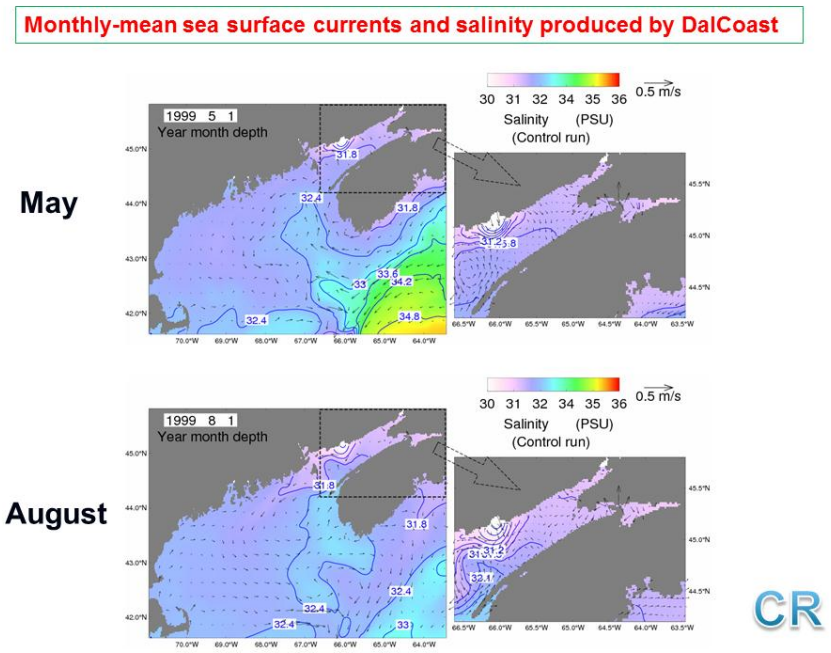

Figure 17. *Monthly mean sea surface salinity in May (upper panels) and August (lower panels) over the BoF, GoM and western SS produced by DalCoast in control run (without tidal in-stream energy extraction, Exp-CR).*

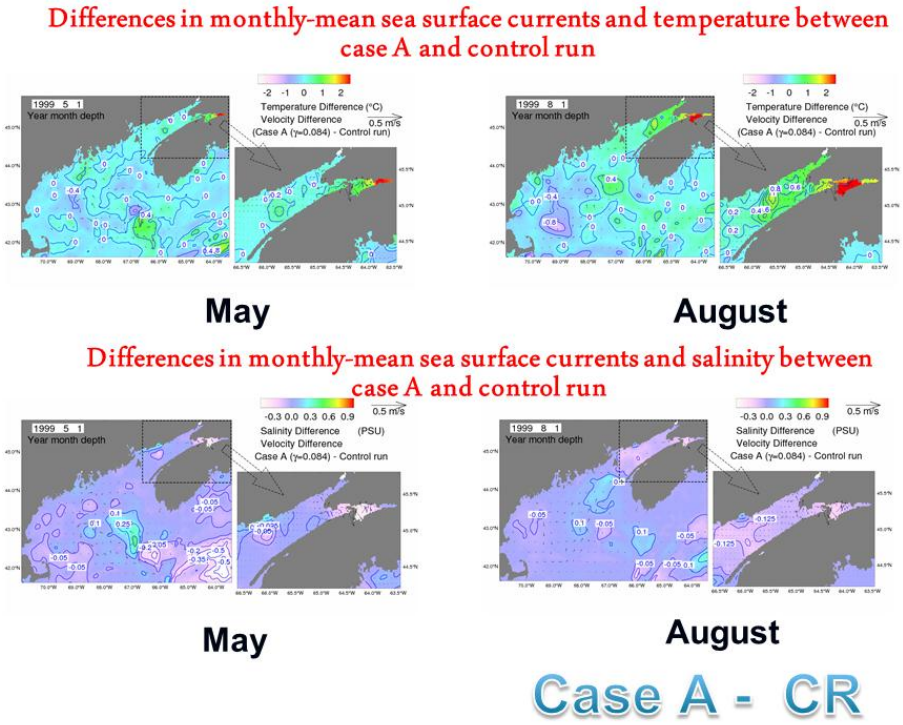

Figure 18. *Differences in monthly mean sea surface temperature (upper panels) and salinity (lower) between Exp-A and Exp-CR in May (left) and August (right) over the BoF, GoM and western SS.*

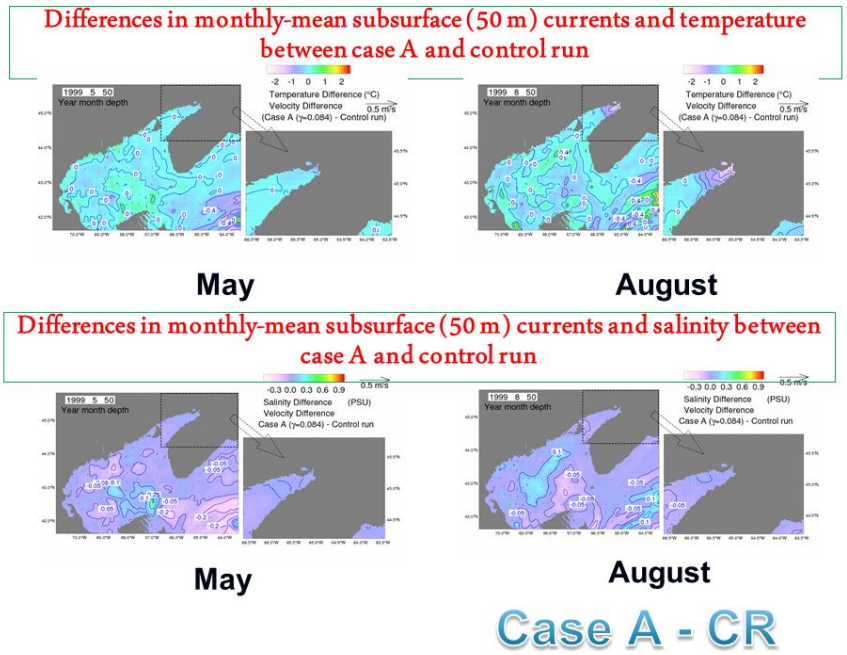

Figure 19. *Differences in monthly mean sub-surface (50 m) temperature (upper panels) and salinity (lower) between Exp-A and Exp-CR in May (left) and August (right) over the BoF, GoM and western SS.*

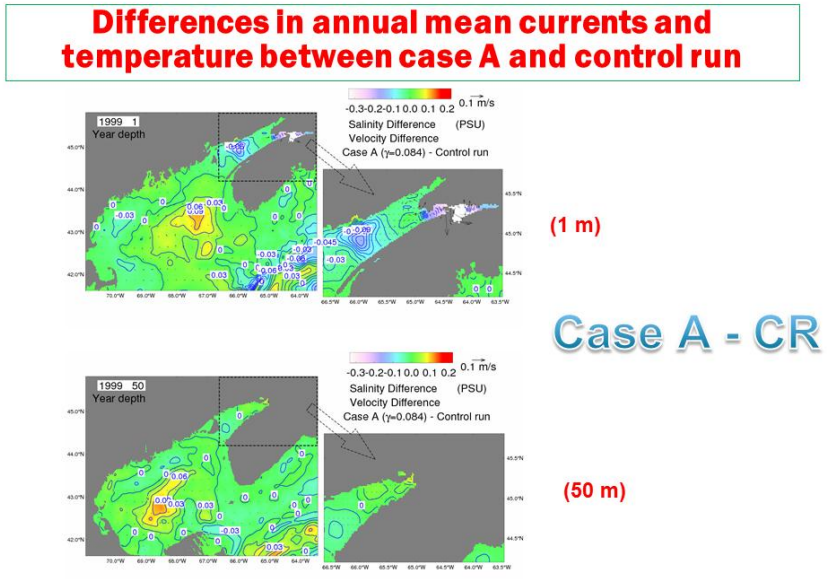

Figure 20. *Differences in annual mean currents, temperature and salinity at depths of 1 m (upper) and 50 m (lower panel) between Exp-A and Exp-CR over the BoF, GoM and western SS.*

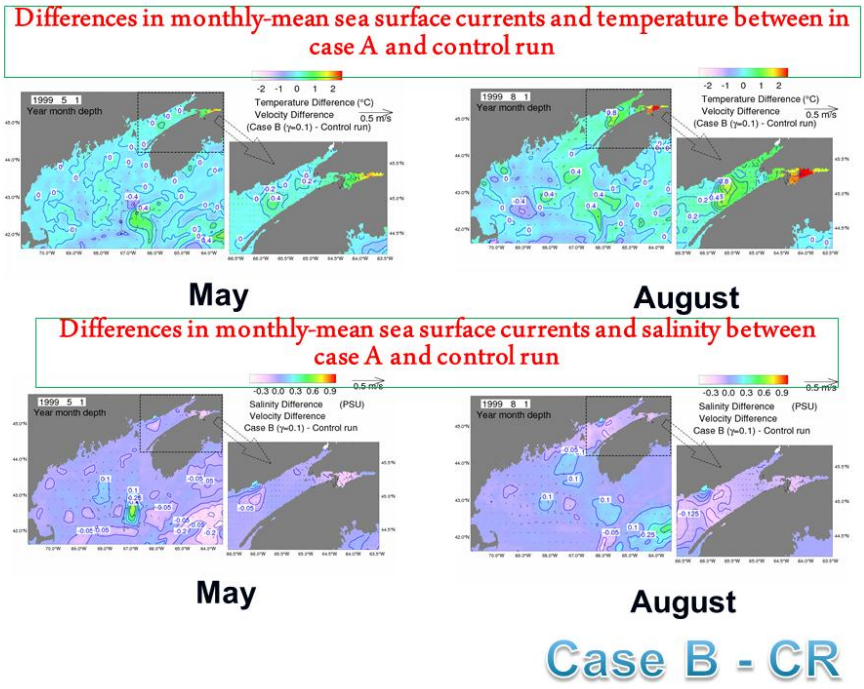

Figure 21. *Differences in monthly mean sea surface temperature (upper) and salinity (lower) in May (left) and August (right) between case B and control run over the BoF, GoM and western SS.*

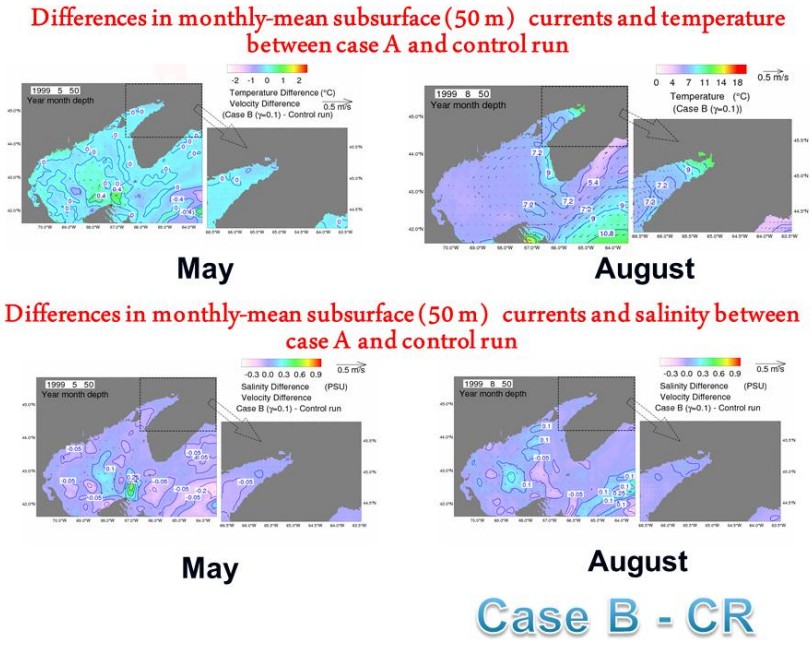

Figure 22. *Differences in monthly mean temperature (upper) and salinity (lower) at 50 m in May (left) and August (right) between Exp-B and Exp-CR over the BoF, GoM and western SS*

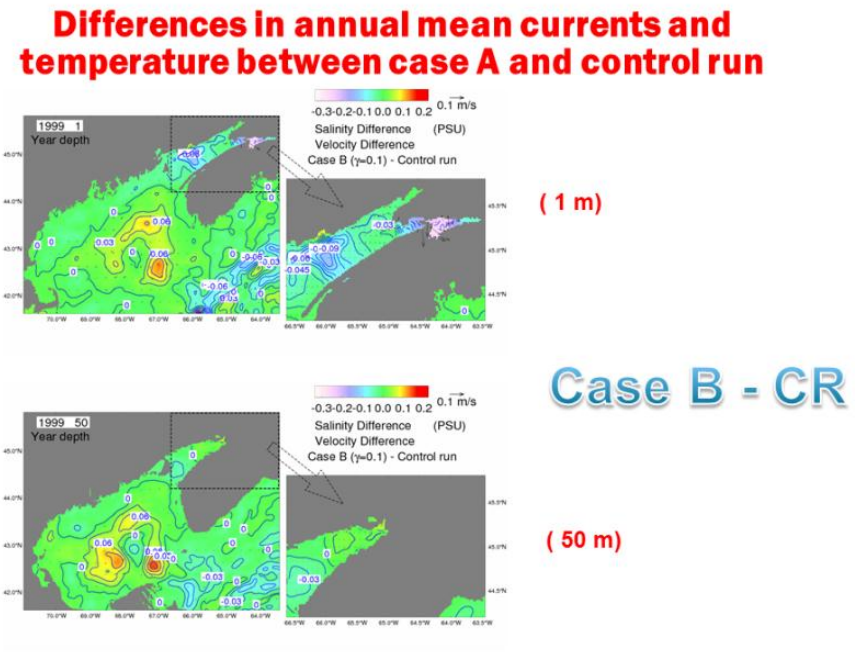

Figure 23. *Differences in annual mean temperature salinity at depths of 1 m (upper) and 50 m (lower panel) between Exp-B and Exp-CR over the BoF, GoM and western SS.*

(c) Far-field effects on sediment distribution in the BoF-GoM region

To examine the far-field effect of the tidal energy extraction in the Minas Passage on the large-scale distribution of bottom sediment in the study region, the bottom sediment properties including the mean, standard deviation, kurtosis and skewness of the sediments were first calculated using the observations taken from various databases including usSEABED database, BIO database, GSC database and CHS bathymetry database. Figure 24 presents the compiled database sample locations with textural class based on mean grain size in the BoF-GoM. Figure 25 presents the interpolated sediment texture distribution over the BoF, GoM and western SS. The bottom sediment types are mainly gravel and sand over the BoF and northwestern GoM, Georges Bank and southwestern SS; and mainly sand and silt over the central and northwestern GoM.

The bottom sediment properties in the study region are affected by many processes, including the hydrodynamics and sediment source. To examine the role of the near-bottom circulation on the bottom sediment types, the maximum bed shear stress (Figure 26) was calculated from the near-bottom maximum tidal currents produced by the nested-grid tidal circulation model in the control run (without tidal in-stream energy extraction in the Minas Passage). A comparison of Figures 25 and 26 demonstrates that the relatively coarse sediment types (gravel and sand) occur over the regions where the maximum bed shear stress is relatively strong, and relatively fine sediment types (sand and silt) occur over the regions where he maximum bed shear stress is relatively weak. It is expected that, if significant tidal in-stream energy is extracted in the BoF,

the bottom sediment types in the region could be modified due to the changes in the maximum bed stress.

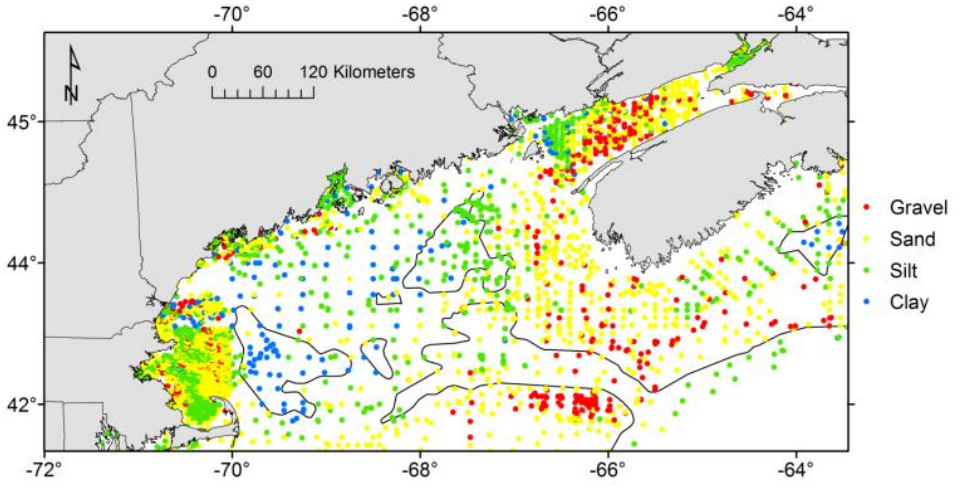

Figure 24. *Compiled database sample locations with textural class based on mean grain size in the BoF-GoM region. The region of the Gulf of Cape Cod and Massachusetts Bay has undergone more sampling than other areas, although the coverage's quality (regularity and resolution of the sampling) is good for most of the BoF-GoM region. The black contour line is that of 200 m depth.*

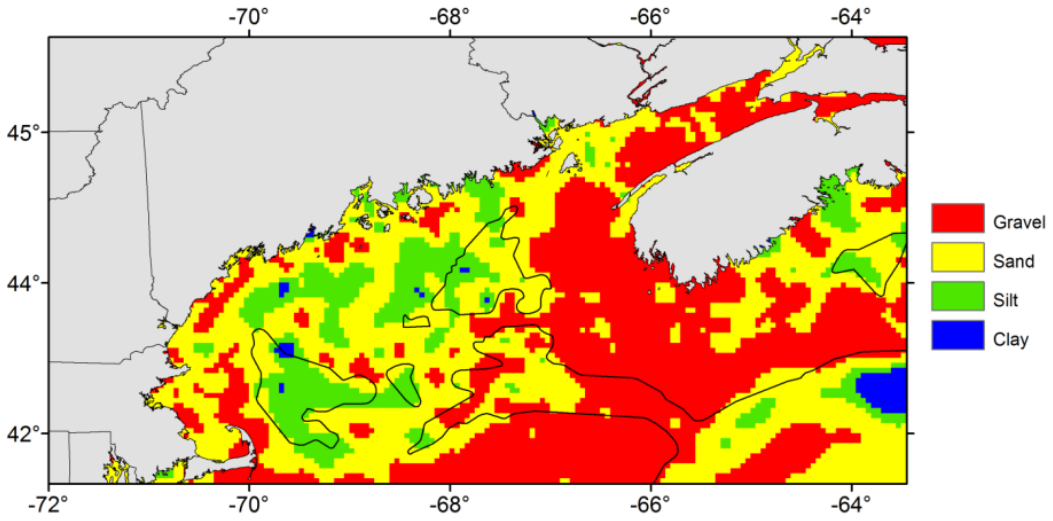

Figure 25. *Sediment texture distribution interpolated using optimal interpolation on a grid with 0.05^o spacing. There are a total of 15,480 data points (172 columns x 90 rows). The black contour lines represent the 200 m isobath.*

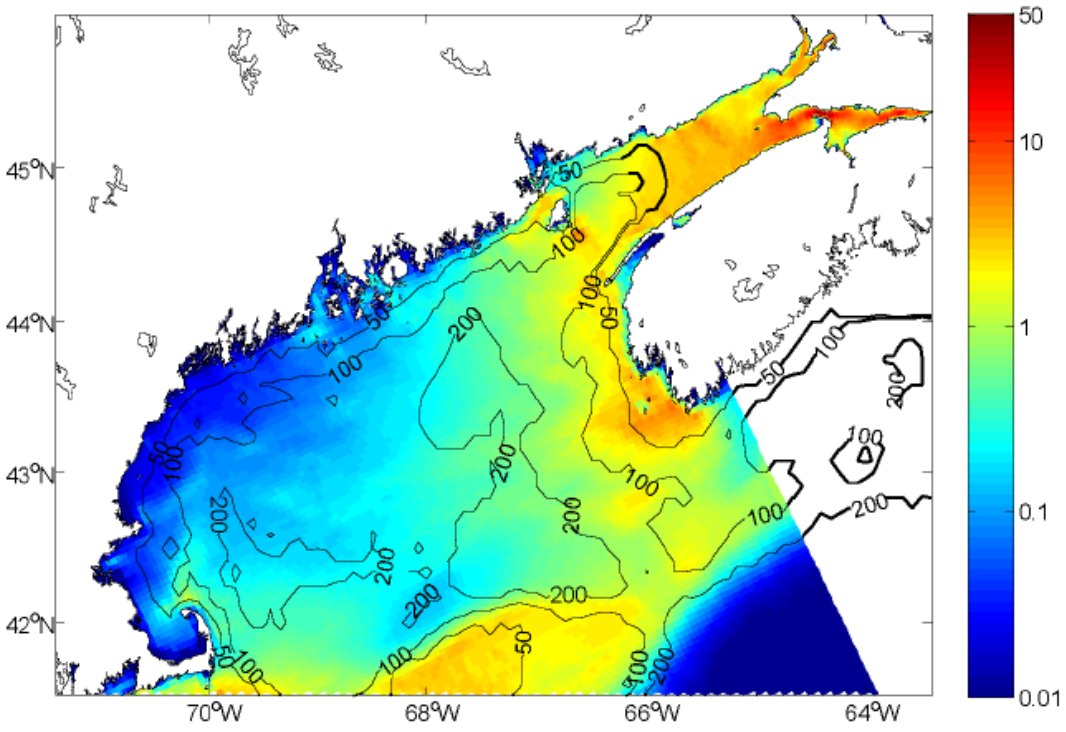

Figure 26. *Maximum bed shear stress (in Pa) calculated from the near-bottom maximum tidal currents in the model run without in-stream tidal energy extraction.*

To demonstrate the effect of the tidal energy extraction in the Minas Passage on the large-scale distribution of the near-bottom sediment types, the differences in the maximum bed shear stress (Figure 27) were calculated from near-bottom tidal currents produced by the tidal circulation models between case A and the control run discussed earlier. As mentioned above, the model results in the control run represent the current ocean state without tidal in-stream energy extraction. The model results in case A represent the ocean state if significant tidal in-stream energy is extracted over the whole water column in the Minas Passage. The changes in the maximum bed shear stress in case A are large over the Minas Passage and adjacent areas where the energy extraction would occur, but relatively small over the GoM, which indicates that the tidal energy extraction in the Minas Passage affects significant the bottom sediment characteristics mainly in the BoF, particularly in the inner BoF.

Figure 28 presents differences in the maximum bed shear stress between case B and the control run discussed earlier. The model results in case B represent the ocean state if the tidal in-stream energy is extracted over the lower water column in the Minas Passage. The large changes in the maximum bed shear stress in case B only occur in the inner BoF, and small over the outer BoF and GoM. Therefore, the effect of the tidal energy extraction on the near-bottom sediment types in case B is mainly limited in the inner BoF and relatively small over other regions.

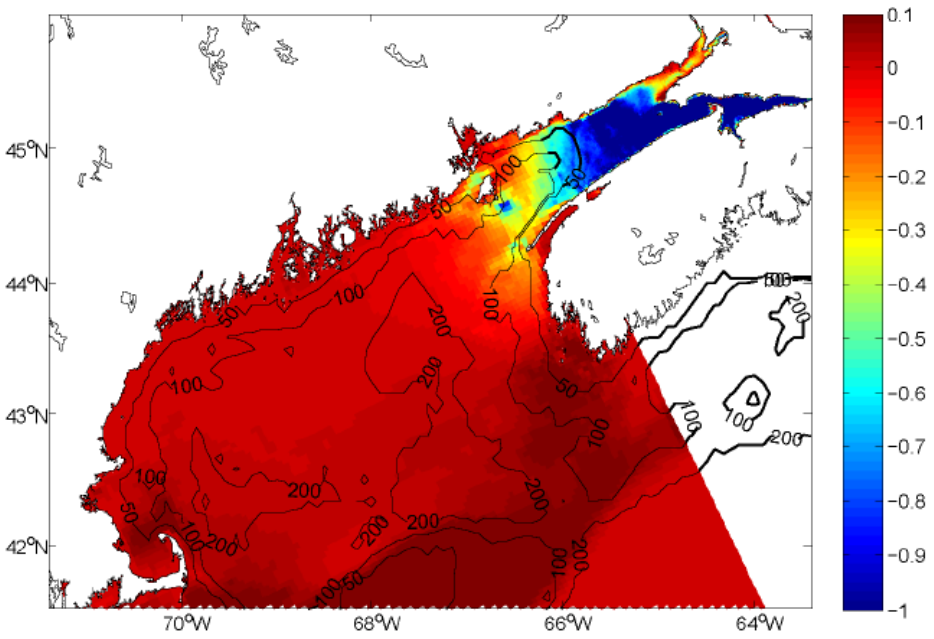

Figure 27. *Differences in maximum bed shear stress (in Pa) calculated from near-bottom tidal currents between case A and the control run.*

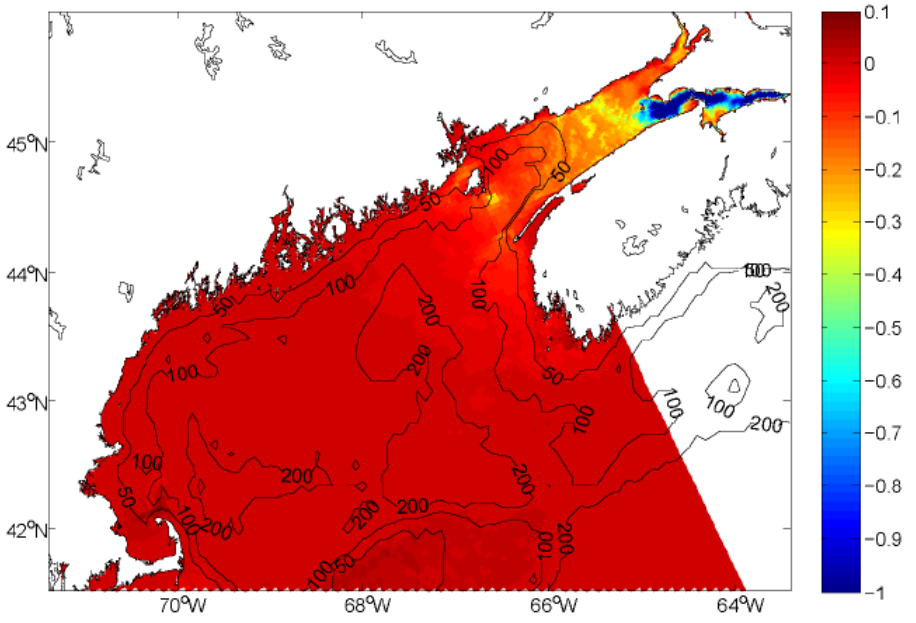

Figure 28. *Differences in maximum bed shear stress (in Pa) calculated from near-bottom tidal currents between case B and the control run.*

Dissemination and Technology Transfer

2010:

Dr. Jinyu Sheng attended an international workshop known as JONSMOD on coastal modeling in Delft of the Netherlands in May, 2010. Many workshop participants are well known scientists in the development and applications of coastal and shelf circulation models. Dr. Sheng made a presentation in the workshop on the development of the two-level nested-grid model for the BOF-GOM region and preliminary model results of tidal circulations in the region. His presentation was well received and he also got constructive and useful suggestions for this research project.

Dr. Daisuke Hasegawa and Dr. Jinyu Sheng attended the annual congress of the Canadian Meteorological and Oceanographic Society (CMOS) in June, 2010. Participants at the congress include professors from Canadian and American Universities and government scientists from the Department of Fisheries and Oceans and Department of Environment Canada. Dr. Hasegawa made an oral presentation on the preliminary numerical study of tidal circulations in the Gulf of Maine and Bay of Fundy with and without tidal energy extraction.

Dr. Jinyu Sheng, Dr. David Greenberg, and Dr. Daisuke Hasegawa attended the OEER/FORCE Tidal Energy Workshop in Wolfville on October 13th, 2010. Dr. Sheng presented our major findings in the first day of the workshop. Dr. Greenberg chaired the session of "Near and Far-Field Effects" on the second day of the workshop.

We were invited by the JONSMOD organizing committee to contribute a peer-reviewed scientific manuscript for a special issue on JONSMOD in the journal of Ocean Dynamics. A manuscript was submitted to the journal in November 2010.

2011:

Dr. Sheng also gave seminars at Hohai University and Southeast University of China respectively in December 2010 and early January 2011 and his talk was well received.

We contributed a newsletter article in Issue 2 of Currents, 2011 and presented our study in the 45th Annual Congress of the Canadian Meteorological and Oceanographic Society.

2012:

Dr. Jinyu Sheng was invited to give a talk at the 4th International Workshop on Modeling the Ocean (IWMO) held in May 2012 in Yokohama, Japan. Most workshop participants are internationally well known scientists in the development and applications of ocean circulation and wave models. Dr. Sheng made a invited presentation in the workshop on the development of two types of shelf circulation models for BoF-GoM region using POM and application of the models in examining the far-field effects of tidal energy extraction on the ocean circulation and hydrography in the BoF-GoM region. His presentation was well received. We were invited by

the IWMO organizing committee to contribute a peer-reviewed scientific manuscript for a special issue in the journal of Ocean Dynamics.

Dr. Jinyu Sheng was also invited to give a talk at the annual congress of the Canadian Meteorological and Oceanography Society held in May 2012 in Montreal, Canada. Attendees of the presentation include scientists from academia and research institutions across Canada. This invited presentation focused mostly on the examination of the far-field effects of tidal energy extraction on the ocean circulation and hydrography in the BoF-GoM region using ocean models. His presentation was well received.

List of conferences, events and meetings attended in which the Research Project and its results were promoted:

1. Sheng, J., and D. Hasegawa, Assessing the far field effects of tidal power extraction on the Bay of Fundy using a nested-grid model, JONSMOD Meeting, Delft, Netherlands, May, 2010.

2. Hasegawa, D., and J. Sheng, Study of tidal circulation and seasonal variability in the Gulf of Maine and Bay of Fundy using a nested-grid ocean circulation model, 44th Annual CMOS Congress, Ottawa, Canada, June, 2010.

3. Sheng, J., and D. Hasegawa, Assessing far field effects of tidal power extraction on the Bay of Fundy, Gulf of Maine and Scotian Shelf, OEER/FORCE Tidal Energy Workshop, Wolfville, October, 2010.

4. Sheng, J., and D. Hasegawa, Assessing far-field effects of tidal power extraction on the Bay of Fundy, Gulf of Maine and Scotian Shelf, Hohai University, Nanjing, China, December, 2010.

5. Sheng, J., and D. Hasegawa, Assessing far-field effects of tidal power extraction on the Bay of Fundy, Gulf of Maine and Scotian Shelf, Southeast University, Nanjing, China January, 2011.

6. Sheng, J., and D. Hasegawa, Investigating far-field effects of tidal in-stream energy extraction in the Minas Passage on tidal circulation in the Bay of Fundy and the Gulf of Maine using a nested-grid coastal ocean circulation model. 45th Annual CMOS Congress, Victoria, Canada, June, 2011.

7. Hasegawa, D., J. Sheng, D. Greenberg, K. Thompson, Investigating far-field effects of tidal energy extraction in the Minas Passage on tidal circulation in the Bay of Fundy and Gulf of Maine using a nested-grid coastal circulation model, Ocean Dynamics, 61, 1845-1868, 2011.

8. Sheng, J., D. Hasegawa, K. Thompson, P. Hill, and D. Greenberg, Assessing the Far Field Effects of Tidal Power Extraction on the Bay of Fundy, Gulf of Maine and Scotian Shelf, Currents (Newsletter of OEER), Issue 2, 2011.

9. Sheng, J., The far-field effect of tidal energy extraction on circulation and hydrography in the Bay of Fundy and Gulf of Maine, 46th Annual CMOS Congress, Montreal, Canada, May, 2012 (invited).

10. Sheng, J., The far-field effect of tidal energy extraction on circulation and hydrography in the Bay of Fundy and Gulf of Maine: Numerical Study using the Princeton Ocean Model, 4th International Workshop on Modelling the Ocean, Yokohama, Japan, May, 2012 (invited).

References

1. Dupont, F, C. Hannah, and D. Greenberg (2005). Modelling the sea level in the upper Bay of Fundy. ***Atmos Ocean*** 43:33–47.

2. Garrett, C., and P. Cummins (2004). Generating power from tidal currents. J***. Waterway Port Coast. Ocean Eng.*** 130:114–118.

3. Geshelin,Y., J. Sheng, and R. Greatbatch (1999). Monthly mean climatologies of temperature and salinity in the western North Atlantic. ***Can. Data Rep. Hydro. Ocean Sci.*** 153: 62 pp.

4. Hasegawa, D., J. Sheng, D. Greenberg, and K. Thompson (2011). Investigating far-field effects of tidal energy extraction in the Minas Passage on tidal circulation in the Bay of Fundy and Gulf of Maine using a nested-grid coastal circulation model, ***Ocean Dyn.*** 61: 1845-1868.

5. Lynch, D., J. Ip, C. Naimie et al. (1996). Comprehensive coastal circulation model with application to the Gulf of Maine. ***Cont. Shelf Res***. 12: 37-64.

6. Ohashi, K., J. Sheng, K. Thompson, C. Hannah and H. Ritchie (2009a). Effect of stratification on tidal circulation over the Scotian Shelf and Gulf of St. Lawrence: a numerical study using a three-dimensional shelf circulation model. ***Ocean Dyn***. 59:809–825.

7. Ohashi, K., J. Sheng, KThompson, C. Hannah, and H. Ritchie (2009b). Numerical study of three-dimensional shelf circulation on the Scotian Shelf using a shelf circulation model. ***Cont. Shelf Res.*** 29: 2138–2156.

8. Petrie, B., B. Topliss, and D. Wright (1987). Coastal upwelling and eddy development off Nova Scotia. J***. Geophys. Res.*** 29:12979–12991.

9. Pettigrew, N., D. Townsend, H. Xue, J. Wallinga, P. Bricldey, and R. Hetland (1998). Observations of the eastern Maine coastal current and its offshore extensions in 1994, ***J. Geophys. Res.*** 103: 30623-30639.

10. Sheng, J., R. Greatbatch, and D. Wright (2001). Improving the utility of ocean circulation models through adjustment of the momentum balance, ***J. Geophys. Res.*** 106: 16711– 16727.

11. Sucsy, P., B. Pearce, and V. Panchang (1993). Comparison of two and three-dimensional model simulation of the effect of a tidal barrier on the Gulf of Maine tides. ***J. Phys Oceanogr.*** 23:1231–1248.

12. Thompson, K., K. Ohashi, J. Sheng, J. Bobanovic, and J. Ou (2007). Suppressing bias and drift of coastal circulation models through the assimilation of seasonal climatologies of temperature and salinity. ***Cont. Shelf Res***. 27:1303–1316.

13. Xue, H., F. Chai, and N. Pettigrew (2000). A model study of the seasonal circulation in the Gulf of Maine. J***. Phys Oceangr.*** 30: 1111-1135.